

Infrared Characterization of Hydroxyl Groups on MgO: A Periodic and Cluster Density Functional Theory Study

Céline Chizallet,^{*,†,#} Guylène Costentin,^{*,†} Michel Che,^{†,§} Françoise Delbecq,[‡] and Philippe Sautet[‡]

Contribution from the Laboratoire de Réactivité de Surface, Université Pierre et Marie Curie-Paris 6, CNRS 4 place Jussieu, 75252 Paris Cedex 05, France, Laboratoire de Chimie, Institut de Chimie de Lyon, Ecole Normale Supérieure de Lyon, CNRS; 46 allée d'Italie, 69364 Lyon Cedex 07, France, and Institut Universitaire de France, 103, bd Saint-Michel, 75005 Paris, France

Received December 5, 2006; E-mail: celine.chizallet@ifp.fr; costenti@ccr.jussieu.fr

Abstract: The infrared OH stretching frequencies of the various types of hydroxyl groups on MgO surfaces have been calculated by periodic (VASP) and cluster (Gaussian) DFT simulations. Surface irregularities (mono and diatomic steps, corners, step divacancies, and kinks) have been considered to model the IR spectra of hydroxylated MgO powders. A good correspondence between calculated and experimental frequencies is obtained with the B3LYP functional. Hydrogen-bonding is the parameter which influences most the IR frequency of OH groups, followed by location of OH groups in concave or convex areas of the surface and then oxygen coordination. The evolution of experimental IR spectra upon evacuation at increasing temperature can be rationalized on the basis of calculated thermal stabilities of each kind of OH groups. A new model is finally proposed to help assign the experimental bands, in terms of hydrogen-bonding, local topology of the hydroxylated sites, and coordination of oxygen.

1. Introduction

Because water is present in many industrial processes, hydroxylation of oxide catalysts has become a most important topic in the surface chemistry of oxides. The interaction of water with solid surfaces and the hydroxyl groups generated have been much studied by infrared (IR) spectroscopy, particularly in the case of acidic catalysts where the vibration frequency is often used to evaluate the proton Brønsted acidity.^{1–8} Recently IR and density functional theory (DFT) data obtained for TiO₂ and γ -alumina nanoparticles^{9–11} have shown that the nature, con-

centration, and thermal stability of hydroxyl groups are related to the particles' morphology and are key parameters which control the acid–base properties and reactivity of oxide surfaces.

Over the last years, solids with basic properties (layered double hydroxides, alkaline exchanged zeolites, alkaline earth oxides, etc.) have attracted much attention and the origin of their basicity has been investigated. In the case of MgO, where surface oxide ions O²⁻_{LC} exhibit low coordination (LC, with L = 3 for corners, 4 for edges, 5 for terraces),¹² morphology is also expected to change the basic properties of hydroxylated surfaces. However, if hydroxyl groups are known to influence the catalytic activity of basic oxides in several systems,^{13–20} their characterization by IR is still a matter of discussion, particularly because of the concomitant existence of carbonates and hydrogen carbonates. For example, on MgO, surface carbonates are still present up to 673 K at pressures below 10⁻³

[†] Université Pierre et Marie Curie.

[‡] Ecole Normale Supérieure de Lyon.

[§] Institut Universitaire de France.

[#] Current address: Institut Français du Pétrole, Direction Chimie et Physico-Chimie Appliquées, 1 et 4 avenue de Bois-Préau, 92852 Rueil-Malmaison Cedex, France.

- (1) Barthelemy, D. *J. Phys. Chem.* **1979**, *83*, 249–256.
- (2) Brunner, E.; Karge, H. G.; Pfeifer, H. *Z. Phys. Chem.* **1992**, *176*, 173–183.
- (3) Sierka, M.; Eichler, U.; Datka, J.; Sauer, J. *J. Phys. Chem. B* **1998**, *102*, 6397–6404.
- (4) Simperler, A.; Bell, R. G.; Anderson, M. W. *J. Phys. Chem. B* **2004**, *108*, 7142–7151.
- (5) Van Santen, R. A.; Kramer, G. J.; Jacobs, W. P. J. H. In *Elementary Reaction Steps in Heterogeneous Catalysis*; Joyner, R. W., Van Santen, R. A., Eds.; Kluwer Academic Publishers: Norwell, MA, 1993; pp 113–131.
- (6) Jeanvoine, Y.; Angyan, J. G.; Kresse, G.; Hafner, J. *J. Phys. Chem. B* **1998**, *102*, 5573–5580.
- (7) Sastre, G.; Fornes, V.; Corma, A. *J. Phys. Chem. B* **2000**, *104*, 4349–4354.
- (8) Gora, A.; Broclawik, E. *J. Mol. Catal. A* **2004**, *215*, 187–193.
- (9) Digne, M.; Sautet, P.; Raybaud, P.; Euzen, P.; Toulhoat, H. *J. Catal.* **2002**, *211*, 1–5.
- (10) Digne, M.; Sautet, P.; Raybaud, P.; Euzen, P.; Toulhoat, H. *J. Catal.* **2004**, *226*, 54–68.

- (11) Arrouvel, C.; Digne, M.; Breyse, M.; Toulhoat, H.; Raybaud, P. *J. Catal.* **2004**, *222*, 152–166.
- (12) Che, M.; Tench, A. J. *Adv. Catal.* **1982**, *31*, 77–133.
- (13) Zhang, G.; Hattori, H.; Tanabe, K. *Appl. Catal.* **1988**, *36*, 189–197.
- (14) Wang, J. A.; Bokhimi, X.; Novaro, O.; Lopez, T.; Gomez, R. *J. Mol. Catal. A* **1999**, *145*, 291–300.
- (15) Kus, S.; Otremba, M.; Torz, A.; Taniewski, M. *Fuel* **2002**, *81*, 1755–1760.
- (16) Bailly, M. L.; Chizallet, C.; Costentin, G.; Krafft, J. M.; Lauron-Pernot, H.; Che, M. *J. Catal.* **2005**, *235*, 413–422.
- (17) Rao, K. K.; Gravelle, M.; Valente, J. S.; Figueras, F. *J. Catal.* **1998**, *173*, 115–121.
- (18) Prinetto, F.; Tichit, D.; Teissier, R.; Coq, B. *Catal. Today* **2000**, *55*, 103–116.
- (19) Climent, M. J.; Corma, A.; Iborra, S.; Vely, A. *J. Mol. Catal. A* **2002**, *182/183*, 327–342.
- (20) Choudary, B. M.; Kantam, M. L.; Reddy, C. R. V.; Rao, K. K.; Figueras, F. *J. Mol. Catal. A* **1999**, *146*, 279–284.

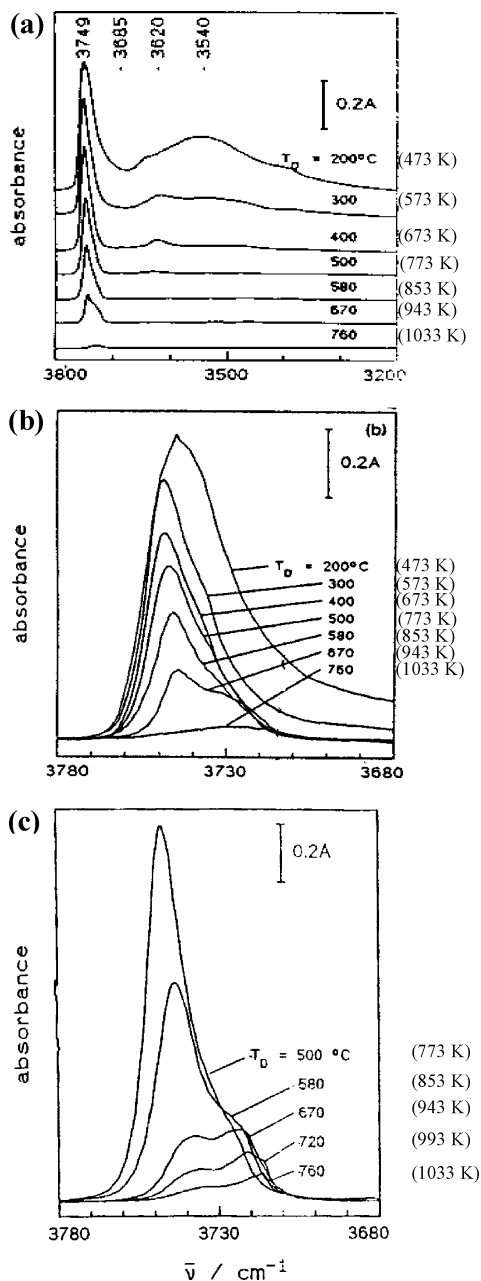


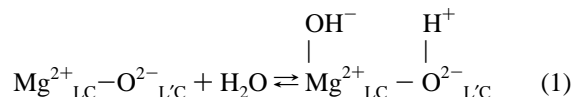
Figure 1. IR spectra of hydroxylated MgO powder (obtained by evacuation at 773 K to remove carbonates followed by hydration and subsequent evacuation in the 473–1033 K range and at 10^{-2} Pa (10^{-4} mbar)), as a function of dehydroxylation temperature, reproduced from ref 22. Panels a and b show sample exhibiting (100) and “high index” planes. Panel c shows sample exhibiting “high index” planes only. The temperatures expressed in degrees Kelvin have been added into brackets.

Pa.²¹ Thus, the study of the O–H stretching frequency region requires decarbonation followed by rehydration.

Typical spectra obtained by Knözinger et al.²² are shown in Figure 1 for a hydroxylated MgO powdered sample, synthesized by CVD (chemical vapor deposition). Similar spectra were obtained by Coluccia et al.,²³ for MgO samples synthesized by in situ decomposition of Mg(OH)₂ under vacuum at 1123 K.

The spectrum at 473 K (Figure 1a) is composed of two main bands: a broad one at low frequency (3200–3650 cm^{-1}) hereafter referred to as the broad band, and a sharp one at high frequency (3650–3800 cm^{-1}) hereafter referred to as the sharp band. Evolution of the spectra upon increasing the temperature under vacuum (Figure 1) shows that (i) both bands contain several components and (ii) the broad band which disappears at about 773 K is less stable.

Two types of hydroxyls are expected to form by heterolytic dissociation of water on $\text{Mg}^{2+}_{\text{LC}}-\text{O}^{2-}_{\text{LC}}$ pairs according to eq 1: those obtained upon protonation of oxide anions $\text{O}^{2-}_{\text{LC}}$ and



those obtained upon hydroxylation of magnesium cations $\text{Mg}^{2+}_{\text{LC}}$.

The IR frequencies are expected to depend on L, L', and hydrogen-bonding. The significant number of types of OH groups explains the composite nature of the two IR bands and the successive models proposed to assign them.

Anderson's Model. This first model,²⁴ completed by Tsyganenko et al.,²⁵ is based on the presence of the two types of OH groups expected from eq 1 and called A, related to hydroxyls on Mg^{2+} , and B, involving O^{2-} ions. The authors considered that on mainly exposed (100) planes, OH groups of type B are closer to the surface, and thus more sensitive to hydrogen-bonding. On this basis, the broad band is assigned to type B hydroxyls, corresponding to $L' = 5$ in eq 1, and the sharp one to “free” type A hydroxyls, with $L = 5$.

Shido's Model. Shido et al.²⁶ refined Anderson's model and distinguished three components within each of the two bands, according to the coordination numbers L and L' in eq 1. Neglecting any shift of the bands caused by hydrogen-bonding, and using an electrostatic model, the authors assigned the sharp band to type A OH groups with

$$\bar{\nu}(\text{Mg}_{5\text{C}}-\text{OH}) > \bar{\nu}(\text{Mg}_{4\text{C}}-\text{OH}) > \bar{\nu}(\text{Mg}_{3\text{C}}-\text{OH})$$

and the broad one to type B hydroxyls with

$$\bar{\nu}(\text{O}_{3\text{C}}-\text{H}) > \bar{\nu}(\text{O}_{4\text{C}}-\text{H}) > \bar{\nu}(\text{O}_{5\text{C}}-\text{H}).$$

Coluccia's Model. The previous models were rejected by Coluccia et al.^{23,27} because the IR bands of types A and B hydroxyls exhibited different thermal stabilities (the stoichiometric removal of water should imply same thermal evolutions for types A and B hydroxyls). Considering the appearance of both frequency domains upon hydrogen^{28,29} and ammonia^{30,31} adsorption, the authors proposed to differentiate the hydroxyls

(21) Mekheimer, G. A. H.; Halawy, S. A.; Mohamed, M. A.; Zaki, M. I. *J. Phys. Chem. B* **2004**, *108*, 13379–13386.
 (22) Knözinger, E.; Jacob, K. H.; Singh, S.; Hofmann, P. *Surf. Sci.* **1993**, *290*, 388–402.
 (23) Coluccia, S.; Marchese, L.; Lavagnino, S.; Anpo, M. *Spectrochim. Acta* **1987**, *43A*, 1573–1576.

(24) Anderson, P. J.; Horlock, R. F.; Olivier, J. F. *Trans. Farad. Soc.* **1965**, *61*, 2754–2762.
 (25) Tsyganenko, A. A.; Filimonov, V. N. *J. Mol. Struct.* **1973**, *19*, 579–589.
 (26) Shido, T.; Asakura, K.; Iwasawa, Y. *J. Chem. Soc. Faraday Trans. 1* **1989**, *85*, 441–453.
 (27) Coluccia, S.; Lavagnino, S.; Marchese, L. *Mat. Chem. Phys.* **1988**, *18*, 445–464.
 (28) Coluccia, S.; Boccuzzi, F.; Ghiotti, G.; Morterra, C. *J. Chem. Soc. Faraday Trans. 1* **1982**, *78*, 2111–2119.
 (29) Knözinger, E.; Jacob, K. H.; Hofmann, P. *J. Chem. Soc. Faraday Trans. 1993*, *89*, 1101–1107.
 (30) Coluccia, S.; Garrone, E.; Borello, E. *J. Chem. Soc., Faraday Trans. 1* **1983**, *79*, 607–613.
 (31) Echterhoff, R.; Knözinger, E. *Surf. Sci.* **1990**, *230*, 237–244.

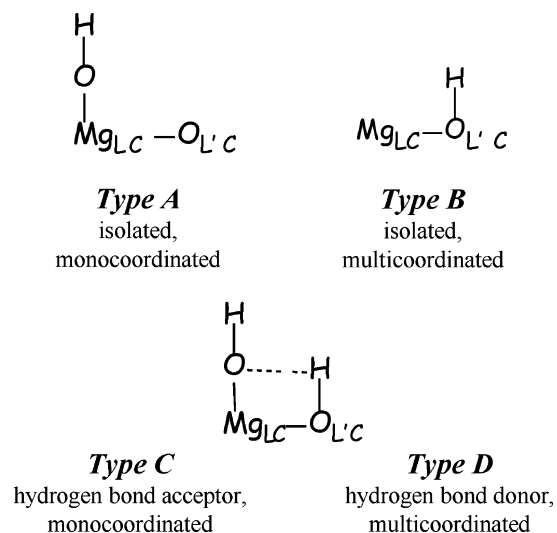


Figure 2. The four types of OH group defined by Knözinger et al.²² to assign their IR spectra.

on the basis of L and L'. OH groups on (100) planes were assumed to be all hydrogen-bonded leading to lower frequency, whatever the hydrogen-bond acceptor or donor nature. This perturbation was thought to be limited for 3C (corners) and 4C (edges) ions. The broad band was thus assigned to hydroxyls with L, L' = 5, and the sharp one to OH on ions of lower coordination, L, L' = 3, 4.

Morrow's Model. Morrow³² pointed out that Coluccia's model was not consistent with the higher intensity of the sharp band for the monolayer coverage. Assuming that hydroxyls Mg_{5C}-OH (L = 5) on (100) planes are less affected by hydrogen-bonding than those involving oxygens (O_{5C}H, L' = 5), he assigned the broad band to the latter hydroxyls and the sharp one to all other OH groups.

Knözinger's Model. On the basis of ammonia adsorption experiments on partially hydroxylated MgO surfaces^{31,33} and of the thermal stability of the bands as a function of sample morphology (Figure 1a–c), Knözinger et al.²² classified the hydroxyls on the basis of hydrogen-bonding into four types (Figure 2). The stretching frequencies of types A and B hydroxyls, assigned for the first time to mono- and multicoordinated hydroxyls, respectively, were both part of the sharp band. Moreover, experimental results and theoretical calculations on small clusters led to assign the high-frequency side (3730–3770 cm⁻¹) of this band to isolated hydroxyls on Mg²⁺ (type A), and the low-frequency side (3710–3730 cm⁻¹) to isolated type B hydroxyls and also to monocoordinated hydrogen-bond acceptor type C hydroxyls. The broad band was assigned to multicoordinated hydrogen-bond donor type D hydroxyls. The various assignments are gathered in Table 1, using the terminology of Knözinger et al.²²

The inconsistency of the models prompted us to systematically study the role of ion coordination, hydrogen-bonding, and, more generally local, environment on the vibrational properties of OH groups.

Computational modeling has become a very powerful tool to help assign IR spectra of OH groups of hydroxylated Al₂O₃

and TiO₂ surfaces.^{10,11,34} Most of the IR studies related to MgO-(100) planes^{35–37} have not taken into account the complex hydration configuration evidenced by other studies.^{38–43} Even when an accurate geometry is used, the theoretical frequencies predicted in the 3550–2500 cm⁻¹ range^{39,40} are much lower than the experimental data,^{44–50} probably because of the use of GGA (generalized gradient approximation) functionals known to overestimate binding energies in hydrogen-bonded systems.^{51–53} TPD results^{42,48,54,55} show that, at 3 × 10⁻⁸ Pa, on MgO(100) terraces at room temperature, no water remains, which is confirmed by calculations, even at 10⁻² Pa:⁵⁶ it thus cannot be involved in the IR bands of Figure 1 and will not be considered in the present work. Irregularities on the MgO surface are thus expected to play an important role in the thermal evolution of the IR spectra.

IR frequencies of water adsorbed on edges or in valleys of steps evaluated earlier^{35,36} lead to two main domains: high wavenumbers are obtained for hydroxyls bonded to Mg²⁺ cations and low frequencies are obtained for protonated oxide ions. Because of the level of calculations,^{35,36} the absolute values obtained are nevertheless not directly comparable to experimental data. Ealet et al.⁵⁷ modeled the hydration of a terrace divacancy, leading to two O_{4C}-H in a very confined environment, and calculated the corresponding frequencies. Although the authors did not quote any absolute value, indication for a strong red-shift compared to free HO⁻ was provided.







It appears there has been no systematic study of the influence of coordination and hydrogen-bonding on stretching frequencies of water adsorbed on irregularities of MgO, described in a realistic way. Water dissociation on steps, corners, and step vacancies was modeled earlier⁵⁶ by a periodic approach (within the density functional theory (DFT) framework and a GGA functional, using the Vienna ab initio simulation package (VASP

- (34) Dzwigaj, S.; Arrouvel, C.; Breyse, M.; Geantet, C.; Inoue, S.; Toulhoat, H.; Raybaud, P. *J. Catal.* **2005**, *236*, 245–250.
- (35) Abdel Halim, W. S.; Shalabi, A. S. *Appl. Surf. Sci.* **2004**, *221*, 53–61.
- (36) Langel, W.; Parrinello, M. *J. Chem. Phys.* **1995**, *103*, 3240–3252.
- (37) Alfredsson, M.; Hermansson, K. *Mol. Simul.* **2002**, *28*, 663–681.
- (38) Giordano, L.; Goniakowski, J.; Suzanne, J. *Phys. Rev. Lett.* **1998**, *81*, 1271–1273.
- (39) Odelius, M. *Phys. Rev. Lett.* **1999**, *82*, 3919–3922.
- (40) Sitte, L. D.; Alavi, A.; Lynden-Bell, R. M. *J. Chem. Phys.* **2000**, *113*, 3344–3350.
- (41) Lynden-Bell, R. M.; Sitte, L. D.; Alavi, A. *Surf. Sci.* **2002**, *496*, L1–L6.
- (42) Kim, Y. D.; Stultz, J.; Goodman, D. W. *J. Phys. Chem. B* **2002**, *106*, 1515–1517.
- (43) Giordano, L.; Goniakowski, J.; Suzanne, J. *Phys. Rev. B* **2000**, *62*, 15406–15408.
- (44) Heidberg, J.; Redlich, B.; Wetter, D. *Ber. Bunsen-Ges. Phys. Chem.* **1995**, *99*, 1333–1337.
- (45) Foster, M.; Furse, M.; Passno, D. *Surf. Sci.* **2002**, *502–503*, 102–108.
- (46) Foster, M.; D'Agostino, M.; Passno, D. *Surf. Sci.* **2005**, *590*, 31–41.
- (47) Hawkins, S.; Kumi, G.; Malyk, S.; Reislser, H.; Wittig, C. *Chem. Phys. Lett.* **2005**, *404*, 19–24.
- (48) Xu, C.; Goodman, D. W. *Chem. Phys. Lett.* **1997**, *265*, 341–346.
- (49) Wu, M. C.; Estrada, C. A.; Corneille, S. A.; Goodman, D. W. *J. Chem. Phys.* **1992**, *96*, 3892–3900.
- (50) Yu, Y.; Guo, Q.; Wang, E.; Möller, P. *J. Phys. Rev. B* **2003**, *68*, 115411–115414.
- (51) Sim, F.; St-Amant, A.; Papai, I.; Salahub, D. R. *J. Am. Chem. Soc.* **1992**, *114*, 4391–4400.
- (52) Mérawa, M.; Civalleri, B.; Ugliengo, P.; Noël, Y.; Lichanot, A. *J. Chem. Phys.* **2003**, *119*, 1045–1052.
- (53) Xu, X.; Goddard, W. A. *J. Phys. Chem. A* **2004**, *108*, 2305–2313.
- (54) Ahmed, S. I.; Perry, S. S.; El-Bjeirami, O. *J. Phys. Chem. B* **2000**, *104*, 3343–3348.
- (55) Johnson, M. A.; Stefanovich, E. V.; Truong, T. N.; Günster, J.; Goodman, D. W. *J. Phys. Chem. B* **1999**, *103*, 3391–3398.
- (56) Chizallet, C.; Costentin, G.; Che, M.; Delbecq, F.; Sautet, P. *J. Phys. Chem. B* **2006**, *110*, 15878–15886.
- (57) Ealet, B.; Goniakowski, J.; Finocchi, F. *Phys. Rev. B* **2004**, *69*, 195411–195419.

(32) Morrow, B. A. *Stud. Surf. Sci. Catal.* **1990**, *57*, 161–222.

(33) Coluccia, S.; Lavagnino, S.; Marchese, L. *J. Chem. Soc., Faraday Trans. 1* **1987**, *83*, 477–486.

Table 1. Assignments of IR Bands in the O–H Stretching Region of Hydroxylated MgO from Various Authors, Using the A, B, C, D Terminology for OH Types from Reference 22 (Figure 2)^a

Authors	Year	References	Assignments
Anderson et al.	1965	24	C with L = 5 D with L' = 5 
Shido et al.	1989	26	A with: B with: L = 5 L = 4 L = 3 L' = 3 L' = 4 L' = 5 
Coluccia et al.	1988	23,27	A, B with L, L' = 3, 4 C, D with L, L' = 5 
Morrow	1990	32	A, B with L, L' = 3, 4 D with L' = 5 
Knözinger et al.	1993	22	A B, C D 
Chizallet et al.	2007	Present work	C A', B, C' D 
Experimental spectrum			$\bar{\nu}(\text{cm}^{-1})$ ← 3800 3650 3200

^a The A' and C' types are proposed in the present work (isolated and hydrogen-bond acceptor O₂C-H, see section 4.3). The white and black rectangles relate to the sharp and broad experimental bands, respectively.

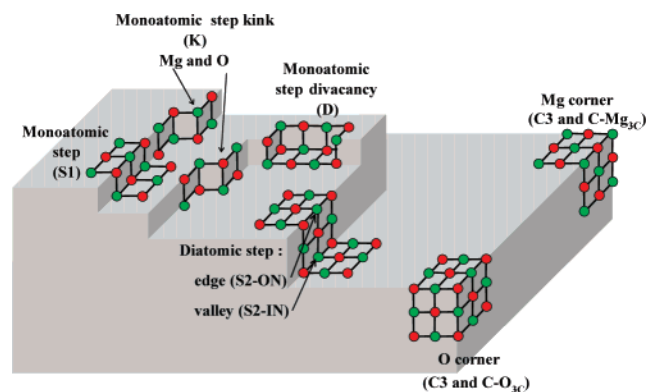


Figure 3. Schematic representation of irregularities on the MgO surface (O²⁻, red spheres; Mg²⁺, green spheres), adapted from Figure 11 of ref 12. The terminologies used for the periodic and cluster systems are given in brackets, see section 2 and ref 56.

code)). The thermal stability of the resulting OH groups was also studied.⁵⁶ The modeled irregularities¹² are schematized in Figure 3.

The aim of the present work is to study how the topology of MgO surfaces and water coverage (depending on temperature) influence the IR spectra and to finally propose one assignment consistent with experimental data. We refine the earlier periodic structures⁵⁶ by building the corresponding clusters, so as to benefit from hybrid functionals (not implemented in VASP yet). Despite that cluster calculations with appropriate embedding schemes have been found to successfully describe the electronic

and adsorptive properties^{58–64} of MgO, a systematic study of water adsorption on realistic defects has never been undertaken. The influence of the coordination number of ions on the stretching frequency can thus be studied. The coverage with water is also varied in periodic systems to study the influence of hydrogen-bonding. The anharmonic vibration frequencies can then be determined, both for periodic and cluster systems.

2. Computational Methods

2.1. Periodic Approach. The methods used, the systems modeled, as well as their hydroxylation and thermodynamic properties were described in a previous work.⁵⁶

2.1.1. Methods. The periodic calculations are performed in the DFT framework and the GGA exchange-correlation functional of Perdew and Wang PW91,⁶⁵ as implemented in VASP 4.6.^{66,67} The one-electron wave function is developed on a basis set of plane waves and the

- (58) Pacchioni, G.; Ricart, J. M.; Illas, F. *J. Am. Chem. Soc.* **1994**, *116*, 10152–10158.
(59) Cai, S.; Neyman, K. M.; Knözinger, H.; Rösch, N. *Surf. Sci.* **2001**, *479*, 169–182.
(60) Sushko, P. V.; Gavartin, J. L.; Shluger, A. L. *J. Phys. Chem. B* **2002**, *106*, 2269–2276.
(61) Diwald, O.; Sterrer, M.; Knözinger, H.; Sushko, P. V.; Shluger, A. L. *J. Chem. Phys.* **2002**, *116*, 1707–1712.
(62) Di Valentin, C.; Giordano, L.; Pacchioni, G.; Rösch, N. *Surf. Sci.* **2003**, *522*, 175–184.
(63) Ricci, D.; Di Valentin, C.; Pacchioni, G.; Sushko, P. V.; Shluger, A. L.; Giamello, E. *J. Am. Chem. Soc.* **2003**, *125*, 738–747.
(64) Chiesi, M.; Giamello, E.; Di Valentin, C.; Pacchioni, G.; Sojka, Z.; Van Doorslaer, S. *J. Am. Chem. Soc.* **2005**, *127*, 16935–16944.
(65) Perdew, J.; Wang, Y. *Phys. Rev. B* **1992**, *45*, 13244–13249.
(66) Kresse, G.; Hafner, J. *Phys. Rev. B* **1994**, *49*, 14251–14269.
(67) Kresse, G.; Furthmüller, J. *Comput. Mat. Sci.* **1996**, *6*, 15–50.

interaction between core and valence electrons is described by the projector augmented waves (PAW) approach.⁶⁸ From preliminary studies on water and its dimer (results not shown), a PAW core radius of 1.52 Å for oxygen and an energy cutoff value of 400 eV were chosen since larger radii (and lower cutoff) overestimate OH bond lengths and underestimate hydrogen-bond length. The convergence criterion for the electronic self-consistent cycle has been fixed at 10^{-6} eV per cell. Geometry optimizations are performed within a conjugate-gradient algorithm until the convergence criterion on forces (10^{-2} eV·Å⁻¹) is reached. The slabs are not symmetrical, which induces a net dipole and consequently a spurious electrostatic interaction between the slab and its periodic images along the z-axis (see ref 56). A dipolar correction along the perpendicular to the slab has been applied to remove this effect. This correction does not exceed 0.05% of the total cohesive energy.

The harmonic O–H stretching wavenumbers $\bar{\nu}_h$ are calculated numerically, with a displacement of ± 0.005 Å around the equilibrium position. Preliminary calculations have shown that the coupling with the surface modes can be neglected, so that only the O and H atoms of hydroxyls are allowed to move. The anharmonicity corrections are performed following the method used by Bates et al.⁶⁹ and Loffreda et al.^{70,71} The potential energy surface is explored manually, by varying the O–H distance in the range ± 0.08 Å so that the first vibrational-state energy is not exceeded, the mass center of the hydroxyl being fixed. A grid of 11 points is used to fit the potential energy variations with a third-order development of the Morse potential, and the anharmonic stretching frequency $\bar{\nu}_{an} = \bar{\nu}_h - \bar{\nu}_{shift}$ is deduced from the resolution of the Schrödinger equation for the Morse potential and from the fit parameters.

2.1.2. Systems and Nomenclature. Among all hydroxyls formed on 4C and 3C ions⁵⁶ considered, only the most stable configurations deduced from a thermodynamic approach performed for a pressure of 10^{-2} Pa (used in Knözinger's experiments²²) are studied here. Moreover, various hydroxyl coverages are considered, with the following nomenclature: system – $n_{ads}W$ (where n_{ads} stands for the number of water molecules per unit cell).

4C ions are modeled by monatomic steps, referred to as S1, and diatomic steps, referred to as S2. Related systems with various hydroxyl coverages include S1, S2-ON and S2-IN (S2 hydroxylated on the edge and in the valley of the step, respectively). For the sake of clarity, the most stable configuration of the monohydrated monatomic step is denoted S1-1w (versus S1-1w-H in ref 56).

3C ions, modeled by the corner systems C3 (large enough to model at the same time Mg^{2+}_{3C} and O^{2-}_{3C} terminated corners⁵⁶) are hydroxylated by one or two water molecules. A single water molecule on C3 can adsorb on either O_{3C}^{2-} or Mg^{2+}_{3C} , leading to C3-1w- O_{3C} and C3-1w- Mg_{3C} configurations, respectively, that finally independently represent the behavior of O^{2-}_{3C} and Mg^{2+}_{3C} terminated corners, respectively. For $n_{ads} = 2$ the most stable configuration consists in the adsorption of two water molecules parallel to the edge linking the corners and is referred to as C3-2w-side.

3C ions in a confined environment are modeled by a divacancy, referred to as D, performed in the edge of S1 and by kinks, called K, performed by formally removing four atoms in the edge of S1. D and K are monohydrated. For D-1w, the most stable configuration corresponds to D-1w- $Mg_{3C}-O_{3C}$, that is, with Mg^{2+}_{3C} hydroxylated and O_{3C}^{2-} protonated. In the case of kinks, K-1w- $Mg_{3C}-O_{4C}$ and K-1w- $Mg_{4C}-O_{3C}$ are the most stable configurations because of the stabilizing bridging of the hydroxyl by three Mg^{2+} ions.

The geometry obtained⁵⁶ was re-optimized using a smaller PAW radius for oxygen and an energy cutoff value of 400 eV to improve the description of the vibrational properties of OH groups.

Table 2. Label, Formula (Mg^* Corresponds to Magnesium Atoms Described by Effective Core Potentials), and Embedding (Number of Point Charges) for the Model Clusters Describing the Various Surface Sites

label	formula	number of embedding charges
S1-1w	$Mg_{20}O_{15}H_2Mg^*_{10}$	2100
S2-ON-1w	$Mg_{10}O_{11}H_2Mg^*_{10}$	1470
S2-IN-1w	$Mg_{22}O_{10}H_2$	913
C-1w- O_{3C}	$Mg_{13}O_{14}H_2Mg^*_{12}$	962
C-1w- Mg_{3C}	$Mg_7O_{10}H_2Mg^*_{10}$	974
D-1w- $Mg_{3C}-O_{3C}$	$Mg_9O_{11}H_2Mg^*_{13}$	2096
K-1w- $Mg_{4C}-O_{3C}$	$Mg_{19}O_{14}H_2Mg^*_9$	2098
K-1w- $Mg_{3C}-O_{4C}$	$Mg_{21}O_{15}H_2Mg^*_{10}$	2091

2.2. Cluster Approach. 2.2.1. Methods. Cluster calculations are performed in the framework of the DFT. The GGA exchange–correlation functional of Perdew and Wang PW91⁶⁵ is used to allow accurate comparison with periodic systems, and the hybrid B3LYP functional^{72,73} is employed to better describe hydrogen-bonded systems. The Gaussian 03⁷⁴ package is used, with Gaussian basis sets. The convergence criterion for the electronic self-consistent cycle is fixed at 10^{-6} Ha ($2.7 \cdot 10^{-5}$ eV) per cluster. Geometry optimizations are performed with the default convergence criteria of Gaussian 03.

In Gaussian 03, harmonic vibrational frequencies are computed by analytic calculation of the second derivative of the energy with respect to the Cartesian nuclear coordinates and then transforming to mass-weighted coordinates. Moreover, anharmonic frequencies are determined by the same methods than those exposed for periodic systems in section 2.1.1.

2.2.2. Systems. Each cluster has its periodic analogue. To limit the size of the cluster, only monohydrated systems are described. In most cases, water atoms, atoms on which water is adsorbed (including those on which bridging of the HO^- ion is formed upon adsorption) and their nearest neighbors are relaxed. The next nearest neighbors are described by a complete Gaussian basis set and were kept fixed during geometry optimization. When next nearest (second order) neighbors are oxygen atoms, their third-order neighbors (magnesium atoms) are described by a LANL2 effective core potential, so as to prevent their artificial polarization by the embedding species.^{75–79} Clusters are embedded in an array of point charges expanded over at least four layers in all directions. The characteristics (terminology, formula, and embedding) of the clusters are given in Table 2. The initial geometry is deduced from the corresponding hydrated periodic system, and further geometry optimization is performed with the functional chosen. Several Gaussian basis sets were compared and the 6-311+G** basis was selected, presenting a good compromise between accuracy and size. The study of size effects on the smallest cluster (C-1w- Mg_{3C}) shows that it allows a fully converged description of O–H bond lengths and converged hydrogen-bond lengths within 0.1%.

3. Results

3.1. Comparison of Periodic and Clusters Systems. As explained earlier for periodic systems,⁵⁶ almost all the defects modeled dissociate water to form hydroxyl groups in a configuration which is surface site dependent. The edge of diatomic

(72) Becke, A. D. *J. Chem. Phys.* **1993**, *98*, 5648–5652.

(73) Lee, C.; Yang, W.; Parr, R. G. *Phys. Rev. B* **1988**, *37*, 785–789.

(74) Frisch, M. J.; et al. *Gaussian 03*, revision C.02; Gaussian, Inc.: Wallingford, CT, 2004.

(75) Sushko, P. V.; Shluger, A. L.; Catlow, C. R. A. *Surf. Sci.* **2000**, *450*, 153–170.

(76) Nygren, M. A.; Pettersson, L. G. M. *J. Chem. Phys.* **1994**, *100*, 2010–2018.

(77) Yudanov, I. V.; Pacchioni, G.; Neyman, K.; Rösch, N. *J. Phys. Chem. B* **1997**, *101*, 2786–2792.

(78) Neyman, K. M.; Rösch, N.; Pacchioni, G. *Appl. Catal. A* **2000**, *191*, 3–13.

(79) Nasluzov, V. A.; Rivanenkov, V. V.; Gordienko, A. B.; Neyman, K. M.; Birkenheuer, U.; Rösch, N. *J. Chem. Phys.* **2001**, *115*, 8157–8171.

(68) Kresse, G.; Joubert, D. *Phys. Rev. B* **1999**, *59*, 1758–1775.

(69) Bates, S.; Dwyer, J. *Chem. Phys. Lett.* **1994**, *225*, 427–430.

(70) Loffreda, D.; Simon, D.; Sautet, P. *Chem. Phys. Lett.* **1998**, *291*, 15–23.

(71) Loffreda, D. Ph.D. Thesis, Ecole Normale Supérieure de Lyon, Université Claude Bernard-Lyon I, 1999.

Table 3. O–H Bond and Hydrogen-Bond Lengths (Å) Calculated for Periodic Systems and Clusters^a

system	Mg _{LC} –O–H				O _{LC} –H				H-bond		
	OH type	periodic PW91	clusters		OH type	periodic PW91	clusters		periodic PW91	clusters	
			PW91	B3LYP			PW91	B3LYP		PW91	B3LYP
S1-											
1w	O _{2C} -H	0.968	0.966	0.959	O _{4C} -H	0.991	0.991	0.976	1.881	1.871	1.950
3w	O _{2C} -H	0.967			O _{4C} -H	0.987			2.034		
S2-ON-											
1w	O _{1C} -H	0.966	0.962	0.955	O _{4C} -H	1.054	1.026	1.002	1.475	1.536	1.590
3w	O _{1C} -H	0.965			O _{4C} -H	1.079			1.420		
	O _{1C} -H	0.965									
S2-IN-											
1w	O _{2C} -H	0.967	0.966	0.958	O _{5C} -H	1.025	1.029	1.004	1.637	1.657	1.733
3w	O _{2C} -H	0.966			O _{5C} -H	1.013			1.737		
C3/C-											
1w-O _{3C}	O _{1C} -H	0.964	0.963	0.956	O _{3C} -H	0.996	0.995	0.980	1.760	1.737	1.805
1w-Mg _{3C}	O _{1C} -H	0.962	0.961	0.954	O _{4C} -H	1.007	1.003	0.985	1.732	1.749	1.840
2w-side	Mg _{4C} -O _{1C} -H	0.964			O _{3C} -H	0.997			1.780		
	Mg _{3C} -O _{1C} -H	0.962			O _{4C} -H	1.006			1.762		
D-											
1w-Mg _{3C} -O _{3C}	O _{3C} -H	0.968	0.966	0.959	O _{3C} -H	0.968	0.965	0.958			
K-											
1w-Mg _{3C} -O _{4C}	O _{3C} -H	0.969	0.968	0.960	O _{4C} -H	0.974	0.973	0.964			
1w-Mg _{4C} -O _{3C}	O _{2C} -H	0.968	0.971	0.961	O _{3C} -H	0.968	0.966	0.958			

^a For S2-ON-3w, the three water molecules are not equivalent. For clusters, only monohydrated systems are considered.

Table 4. Anharmonic Frequencies (cm⁻¹) of OH Groups Calculated for Periodic Systems and Clusters.

system	OH type	Mg _{LC} –O–H		OH type	O _{LC} –H	
		$\bar{\nu}_{\text{an}}$ (cm ⁻¹)			$\bar{\nu}_{\text{an}}$ (cm ⁻¹)	
		periodic PW91	clusters B3LYP		periodic PW91	clusters B3LYP
S1-						
1w	O _{2C} -H	3652 (157)	3781 (127)	O _{4C} -H	3144 (214)	3418 (172)
3w	O _{2C} -H	3685		O _{4C} -H	3266	
S2-ON-						
1w	O _{1C} -H	3693 (160)	3843 (126)	O _{4C} -H	1822 (428) ^b	2798 (274)
3w	O _{1C} -H	3704		O _{4C} -H	2407	
	O _{1C} -H	3699		O _{4C} -H	1622	
S2-IN-						
1w	O _{2C} -H	3692 (139)	3786 (129)	O _{5C} -H	2453 (312)	2819 (248)
3w	O _{2C} -H	3703		O _{5C} -H	2675	
C3/C-						
1w-O _{3C}	O _{1C} -H	3713 (160)	3821 (128)	O _{3C} -H	3047 (226)	3330 (180)
1w-Mg _{3C}	O _{1C} -H	3749 (168)	3861 (128)	O _{4C} -H	2832 (247)	3194 (240)
2w-side	Mg _{4C} -O _{1C} -H	3715		O _{3C} -H	3053	
	Mg _{3C} -O _{1C} -H	3753		O _{4C} -H	2864	
D-						
1w-Mg _{3C} -O _{3C}	O _{3C} -H	3657 (174)	3792 (124)	O _{3C} -H	3656	3808
K-						
1w-Mg _{3C} -O _{4C}	O _{3C} -H	3643 (163)	3768 (129)	O _{4C} -H	3548 (162)	3699 (130)
1w-Mg _{4C} -O _{3C}	O _{2C} -H	3654 (146)	3738 (129)	O _{3C} -H	3661 (163)	3792 (128)

^a Anharmonic shifts are reported in parentheses. Frequencies reported in bold are calculated according to the method given in section 2.1.1. The other ones are deduced from the value of $\bar{\nu}_{\text{shift}}$ calculated for the monohydrated analogues. For clusters, only monohydrated systems are considered. ^b This very low value is explained by strong coupling with H–O–H bending modes, insofar as the adsorbed water molecule is only slightly dissociated. This effect is less pronounced with the B3LYP functional, which leads to enhanced dissociation compared to PW91. This explains the significant difference between PW91 and B3LYP results for S2-ON-1w.

steps (S2-ON) is the defect where dissociation is the most difficult, as shown by a very strong hydrogen-bonding between the resulting proton and hydroxyl. On other systems, contrary to expectation, monocoordinated OH groups are not always formed (Figure 2), but hydroxylation of Mg²⁺_{LC} also provides O_{2C}–H (S1 for instance) and O_{3C}–H (for D and K) when bridging between several Mg²⁺_{LC} is possible.

These results are confirmed by the cluster approach, whatever the functional used. O–H bond and hydrogen-bond lengths are given in Table 3. The proton and hydroxyl issued from water

dissociation are generally hydrogen-bonded, except for D and K, where isolated OH groups are obtained.

Clusters optimized within the PW91 functional exhibit almost the same geometry as their periodic analogues (maximum differences: 0.4% for hydrogen-bond acceptor OH groups, 2.7% for hydrogen-bond donor OH groups, 4.1% for hydrogen-bonds), thus validating the structure chosen for the clusters. However, use of the B3LYP functional systematically leads to shorter O–H bonds (by 2.5%) and longer hydrogen-bond (by 5.2%) compared to clusters optimized within the PW91

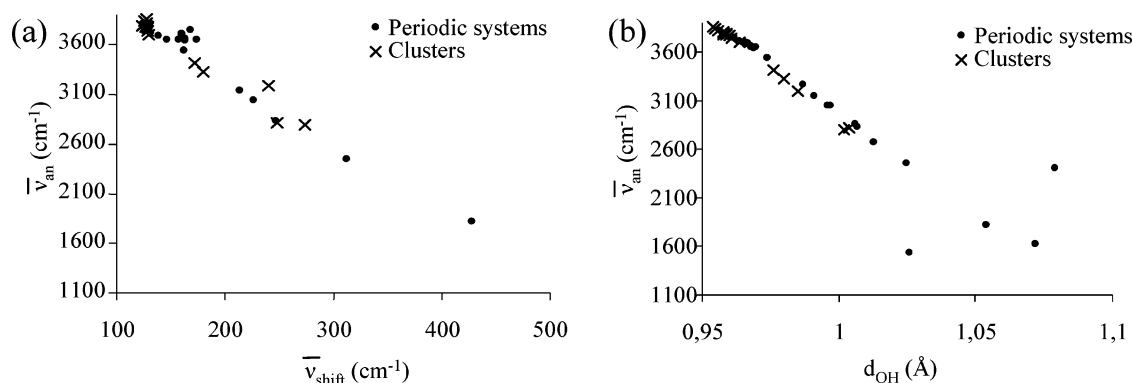


Figure 4. For all considered hydroxylated structures, plots of (a) the anharmonic frequency as a function of anharmonic shift; (b) the anharmonic frequency as a function of O–H bond length. Periodic systems are considered with the PW91 functional, and cluster models are considered with the B3LYP functional.

functional. This corresponds to the description of weak interactions more accurate by hybrid functionals than by GGA, in line with literature data for hydroxyls of a wide range of solid compounds^{52,80–85} and in the study of the water and its dimer (results not reported). For all hydrogen-bonded systems, d_{OH} is larger for hydrogen-bond donor hydroxyls than for hydrogen-bond acceptor hydroxyls, in line with earlier data.^{86,87}

The periodic approach allows a study of the influence of the coverage of the surface with water. Surprisingly, for S1, S2-IN, and C3, increasing the coverage induces a decrease of O–H bond lengths and an increase of the hydrogen-bond length. In fact, increasing the water content leads to water dissociation in a more symmetrical way, insofar as a proton has a higher probability to be surrounded by two nearly equivalent hydroxyls, coming from two different water molecules, as witnessed by the weakening in hydrogen-bonding (Table 3). Such effect is however not observed, and even opposite, on S2-ON.

This could mean that the edge of diatomic steps is not dissociating enough to enable the formation of the more symmetrical structure observed for S1-3w. Steric hindrance between adsorbed water molecules, or screening of the Madelung field induced by other ions on the edge may prevail over symmetry, leading to strengthening of hydrogen-bonding as the coverage increases.

Except for the hardly dissociating S2-ON-1w system, harmonic frequencies calculated for periodic systems and clusters optimized within the PW91 functional (not shown) are in good agreement (difference from 0.1 to 2.4%). This further validates the structure chosen for the clusters. Consistent with shorter O–H bonds, harmonic frequencies are larger with B3LYP than with PW91.

3.2. Anharmonic Frequencies. The harmonic frequencies related to hydrogen-bond donor OH groups calculated thanks to PW91 (periodic and clusters) are largely underestimated (2050–3480 and 2714–3375 cm^{-1} for periodic systems and

clusters, respectively) in comparison to experimental anharmonic stretching frequencies (greater than 3200 cm^{-1}). On the contrary, the greater values obtained with B3LYP show that a better fit with experimental data is expected from calculation of anharmonic shifts using this functional for clusters, given in Table 4. Anharmonic frequencies obtained with this method for periodic systems are also given for the sake of comparison and to identify the influence of the coverage with water (not studied with the cluster approach).

The order of magnitude of calculated anharmonicity shifts is in line with data either calculated^{35,81,82,85,88–91} or experimentally obtained⁹² for various OH-containing solids (to the best of our knowledge, no experimental anharmonicity shifts measurements have ever been reported for MgO). Anharmonicity shifts markedly depend upon the nature of the OH group: hydrogen-bond donor OH groups all exhibit higher anharmonic shifts than hydrogen-bond acceptors or isolated OH groups. Inside each category of hydroxyls, there is no clear influence of oxygen coordination on anharmonic shift. Comparison of K-1w-Mg₃C–O₄C and K-1w-Mg₄C–O₃C leads to

$$\bar{\nu}_{\text{shift}}(\text{O}_{4\text{C}}-\text{H}) \approx \bar{\nu}_{\text{shift}}(\text{O}_{3\text{C}}-\text{H}) \approx \bar{\nu}_{\text{shift}}(\text{O}_{2\text{C}}-\text{H})$$

The anharmonic frequency is rather correlated to $\bar{\nu}_{\text{shift}}$ itself, as evidenced by Figure 4a, despite a quite scattered distribution above 3600 cm^{-1} .

Anharmonic frequencies are almost linearly correlated to O–H distances (Figure 4b) as obtained for a wide range of compounds,^{93,94} showing that the stretching frequency, and thus the anharmonicity shift, are closely linked to the OH bond strength. Note that the variation to linear behavior observed for two points related to S2-ON-3w (Figure 4b) is probably due to the strong coupling between the stretching and bending vibration modes observed in this particular case.

4. Discussion

4.1. Parameters Governing the Stretching Frequencies. Anharmonic stretching frequencies for each kind of system are

(80) O'Malley, P. J.; Farnworth, K. J. *J. Phys. Chem. B* **1998**, *102*, 4507–4515.
 (81) Baranek, P.; Lichanot, A.; Orlando, R.; Dovesi, R. *Chem. Phys. Lett.* **2001**, *340*, 362–369.
 (82) Ugliengo, P.; Pascale, F.; Mérawa, M.; Labéguerie, P.; Tosoni, S.; Dovesi, R. *J. Phys. Chem. B* **2004**, *108*, 13632–13637.
 (83) Pascale, F.; Tosoni, S.; Zicovich-Wilson, C.; Ugliengo, P.; Orlando, R.; Dovesi, R. *Chem. Phys. Lett.* **2004**, *396*, 308–315.
 (84) Tosoni, S.; Doll, K.; Ugliengo, P. *Chem. Mater.* **2006**, *18*, 2135–2143.
 (85) Farnworth, K. J.; O'Malley, P. J. *J. Phys. Chem.* **1996**, *100*, 1814–1819.
 (86) Goniakowski, J.; Noguera, C. *Surf. Sci.* **1995**, *330*, 337–349.
 (87) Costa, D.; Chizallet, C.; Ealet, B.; Goniakowski, J.; Finocchi, F. *J. Chem. Phys.* **2006**, *125*, 054702–054710.

(88) Raybaud, P.; Digne, M.; Ifimie, R.; Wellens, W.; Euzen, P.; Toulhoat, H. *J. Catal.* **2001**, *201*, 236–246.
 (89) Arrouvel, C.; Toulhoat, H.; Breyse, M.; Raybaud, P. *J. Catal.* **2004**, *226*, 260–272.
 (90) Sillar, K.; Burk, P. *Chem. Phys. Lett.* **2004**, *393*, 285–289.
 (91) Mihaleva, V. V.; Van, Santen, R. A.; Jansen, A. P. J. *J. Chem. Phys.* **2004**, *120*, 9212–9221.
 (92) Kustov, L. M.; Borovkov, V. Y.; Kazansky, V. B. *J. Catal.* **1981**, *72*, 149–159.
 (93) Novak, A. *Struct. Bonding (Berlin)* **1974**, *18*, 177–216.
 (94) Lutz, H. D. *Struct. Bonding* **1988**, *69*, 97–125.

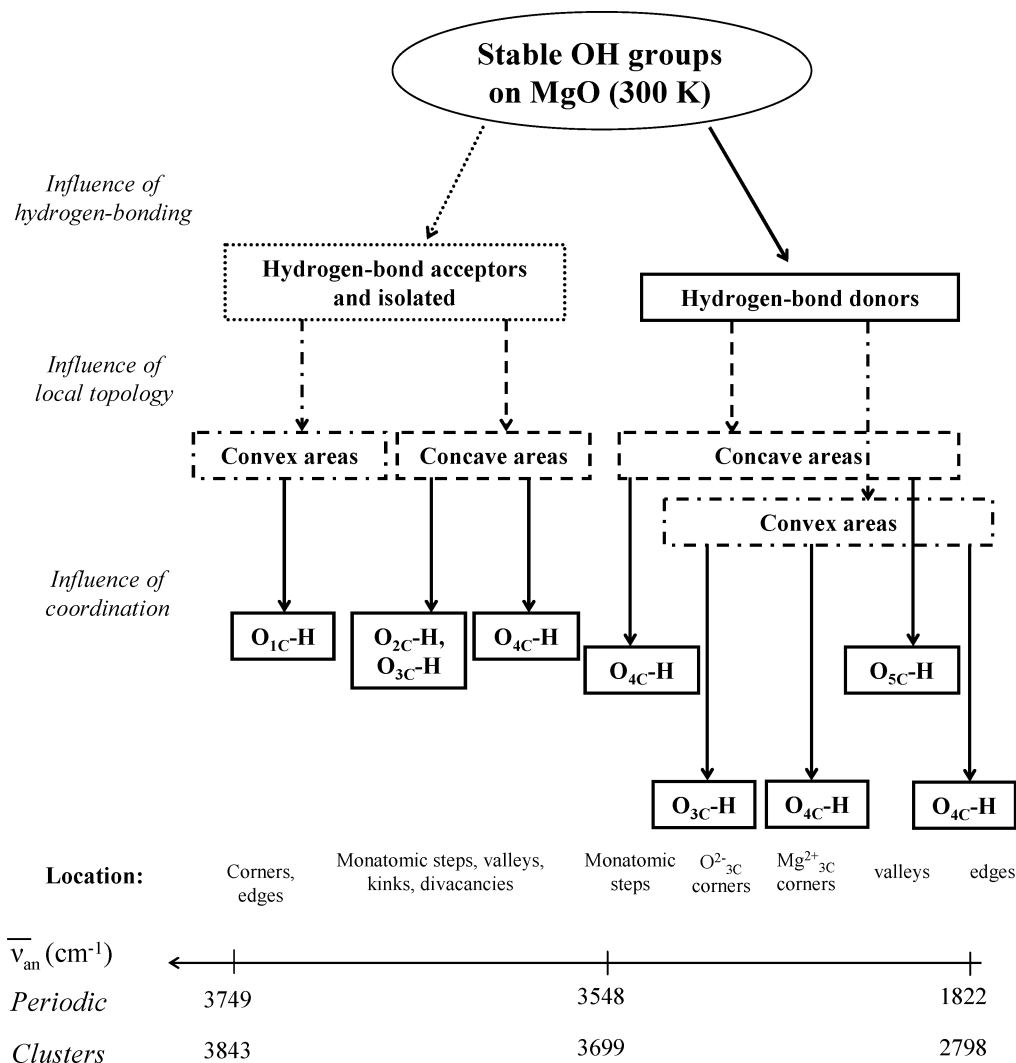


Figure 5. Diagram showing the influence of hydrogen-bonding, local topology (concave or convex), and oxygen coordination on the calculated stretching frequency of OH groups for MgO (monohydrated systems only). The first set of values refers to periodic calculations with the PW91 functional, and the second refers to cluster results with the B3LYP functional.

summarized in Figure 5. The influence of factors involved in determining the stretching frequency of a given OH group is shown as a function of the interplay existing with its environment (hydrogen-bonding, interaction with the lattice in concave areas, coordination). For the sake of clarity, only monohydrated systems are represented.

Hydrogen-bonding is the parameter which influences most the stretching frequency, as discussed above for anharmonic shifts.^{93,94} Hydroxyl groups fall into two categories: hydrogen-bond donors at lower frequencies and other hydroxyl groups at higher frequencies. Frequencies of hydrogen-bond donors depend more upon hydrogen-bonding than hydrogen-bond acceptors (see in Table 4 the differences of 404 and 281 cm^{-1} in periodic and clusters systems, respectively, for O_{4C}-H in S1-1w and K-1w-Mg_{3C}-O_{4C} compared to the small differences between O_{2C}-H in S1-1w and K-1w-Mg_{4C}-O_{3C}).

These results are in line with Anderson's²⁴ and Morrow's³² models, restricted however to (100) plane of MgO (site of low coordination sites were not considered). Although they considered the influence of hydrogen-bonding on the stretching frequency, Coluccia et al.^{23,27} did not discuss the donor/acceptor character of hydrogen-bonding. Most authors emphasized the role of isolated OH groups. Shido et al.²⁶ did not take into

account the existence of hydrogen-bonding. Coluccia et al.^{23,27} and Knözinger et al.²² assigned the higher frequency band to isolated OH groups.

The present work shows that (i) isolated hydroxyls are observed only on kinks and step divancies, whereas hydrogen-bonding is present in all other cases; (ii) their frequency which belongs to the high frequency domain, as predicted by Coluccia et al.^{23,27} and Knözinger et al.,²² is often lower than for hydrogen-bond acceptor OH groups, a result which is quite unexpected.

Isolated and hydrogen-bond acceptor OH groups can be distinguished on the basis of their location in concave or convex areas (defined earlier⁵⁶ as reproduced in Figure 6).

Indeed, owing to the possibility of bridging in concave areas (formation of O_{3C}-H and O_{2C}-H for D and K, and of O_{2C}-H for S1 and S2-IN), isolated and hydrogen-bond acceptor OH groups interact more strongly with their environment resulting in lower frequencies than those for hydrogen-bond acceptor O_{1C}-H in convex areas (C3 and S2-ON). Moreover, inside each category (concave or convex), the stretching frequency of hydrogen-bond acceptor and isolated OH groups increases as the coordination number of oxygen of the hydroxyl decreases: $\bar{\nu}(\text{O}_{1\text{C}}-\text{H}) > \bar{\nu}(\text{O}_{2\text{C}}-\text{H}) \approx \bar{\nu}(\text{O}_{3\text{C}}-\text{H}) > \bar{\nu}(\text{O}_{4\text{C}}-\text{H})$.

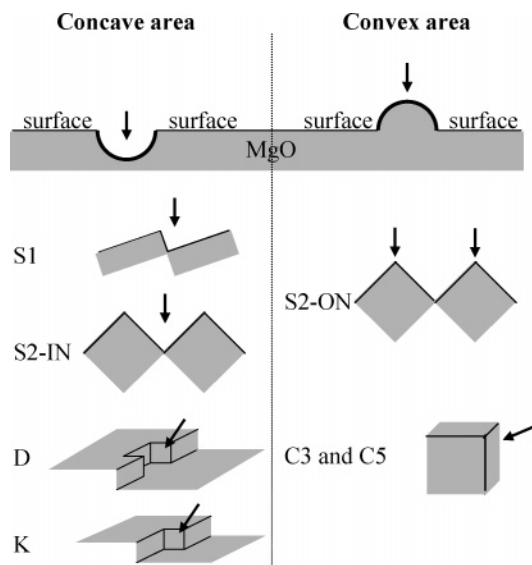


Figure 6. Schematized representation of concave and convex areas: general case (top) and examples. Arrows depict the surface area where water adsorption takes place. (Reproduced from Figure 8 of ref 56).

However, comparison of $O_{2C}-H$ for S1-1w with $O_{3C}-H$ for D1w-Mg_{3C}-O_{3C} indicates that the influence of hydrogen-bonding prevails over oxygen coordination on the OH frequency.

For hydrogen-bond donor OH groups, the coordination of oxygen and their location (concave/convex areas) act now as two competing parameters. As a matter of fact, the location no longer prevails over the coordination of oxygen, as exemplified by the lower frequency of $O_{5C}-H$ for S2-IN-1w (concave) than that of $O_{4C}-H$ for C₃/C-1w-Mg_{3C} (convex). In fact, hydrogen-bond donor OH groups interact more weakly with the corresponding hydrogen-bond acceptor in concave areas than in convex areas as shown, for example, by hydrogen-bond length of $O_{4C}-H$ for S1-1w and C₃/C-1w-Mg_{3C} in Table 3. As a result, the hydrogen-bond donor OH groups globally exhibit slightly higher frequencies in concave areas than in convex areas.

Finally, the influence of water coverage can be discussed on the basis of periodic studies. The effect on frequencies is similar to the one already given on distances in section 3.1. Because of the symmetry effect, the anharmonic frequency increases with coverage for S1 and C₃/C and more slightly for S2-IN and for the $O_{1C}-H$ for S2-ON. This effect is unexpected at first sight, insofar as the increase of coverage is expected to increase the occurrence of hydrogen-bonding leading to lower values in frequencies. The only exception is the $O_{4C}-H$ of the S2-ON system which is probably not dissociating enough. These features should not be generalized to higher water pressures, where nondissociated molecules adsorbed on hydroxyls under study could change this trend.

4.2. Comparison of Theoretical Results with Experimental Data. **4.2.1. Frequency Ranges.** To compare the theoretical results with experimental data (Figure 1), it is first important to determine which OH species exist at 473 K under a water pressure of 10^{-2} Pa, on the basis of previous work.⁵⁶ The corresponding simulated spectra obtained at 473 K with the clusters approach with the B3LYP functional are shown in Figure 7. The results obtained with the PW91 functional (for either cluster or periodic systems) only differ by the absolute values of the calculated stretching frequency, the relative band positions being similar.

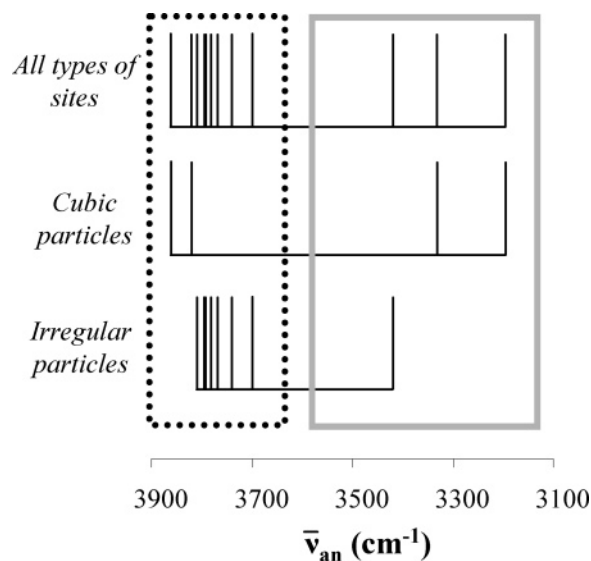


Figure 7. Simulated IR spectra (cluster approach, B3LYP) for a MgO powder hydroxylated at a water pressure of 10^{-2} Pa and at 473 K. Surface sites present on cubic particles or on very irregular particles are displayed independently. The dotted box encloses the sharp band and the gray one the broad band.

The (100) planes, the edges S2-ON, and valleys S2-IN being fully dehydrated at 473 K, the frequencies of hydrogen-bonded donor OH groups (2798 and 2819 cm^{-1} for B3LYP cluster models, respectively) are not observed. Two main groups appear at high ($\bar{\nu}_{\text{an}} = 3699\text{--}3861$ cm^{-1} for B3LYP clusters) and low frequency ($\bar{\nu}_{\text{an}} = 3194\text{--}3418$ cm^{-1} for B3LYP clusters). This agrees rather well with experimental data and confirms the existence of irregularities on real MgO samples. The shift of the broad band to lower frequencies compared to the experimental broad band can be explained by the overestimation of the strength of hydrogen bonds due to DFT, as reported earlier.³⁶

The morphology of the sample greatly influences the shape of the spectrum as shown by the comparison of the high-frequency bands presented on Figure 1 panels a and b ((100) planes and high index planes, according to Knözinger et al.²²), and Figure 1c (“high index planes” only). Perfect cubic particles are expected to exhibit only terraces, edges (depicted by S2-ON), and corners (C₃/C), whereas samples with irregularities should mainly exhibit monatomic steps, valleys, kinks, and divancies. These expectations are confirmed by Figure 7 which predicts that the low-frequency side of the sharp band is more intense on the irregular powder than on the regular one, in line with experimental spectra near 3725 cm^{-1} (Figure 1b,c). The present model thus enables an explanation of the differences in shapes of the sharp band of morphologically different samples (Knözinger et al.²² did not give any experimental data on the broad band).

4.2.2. Thermal Evolutions. Calculated stretching frequencies can be plotted as a function of temperature insofar as the stability of each system is known from thermodynamic calculations.⁵⁶ The expected spectra are given in Figure 8. Most experimental data (Figure 1) can be explained theoretically (Figure 8).

Indeed, the broad band ($3200\text{--}3650$ cm^{-1}) experimentally disappears at lower temperature than the sharp band at high frequency. This fact is well predicted by calculations, although at lower temperature than experimentally (610 instead of 773 K). Moreover, above 573 K, the experimental shift of the sharp

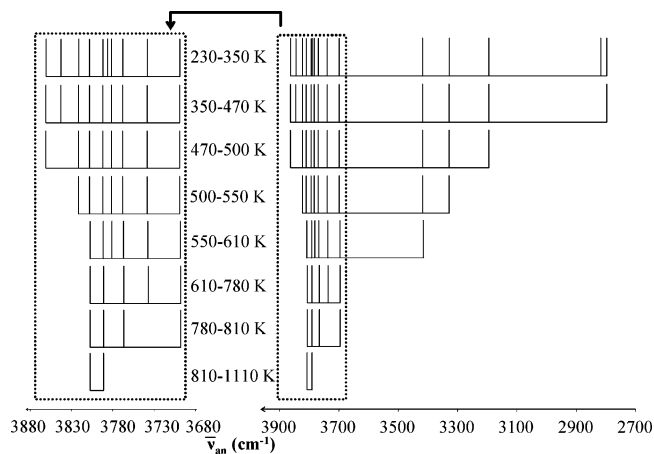


Figure 8. Simulated IR spectra (cluster approach, B3LYP) of hydroxylated MgO powder as a function of temperature, for $P = 10^{-2}$ Pa. The inset on the left shows an extended view of the sharp band at high frequency.

band from 3750 to 3725 cm^{-1} , as the temperature increases, can be explained by (i) the decrease of the $\text{O}_{2\text{C}}\text{-H}$ frequency on monatomic steps S1 with coverage, and (ii) the disappearance of $\text{O}_{1\text{C}}\text{H}$ on edges and corners at lower temperature than OH groups on kinks and divacancies, leading to lower frequencies. However, the high-frequency side of the sharp band is expected to disappear near 550 K from calculations, whereas it is observed between 943 and 1033 K experimentally: only qualitative trends can be expected from calculations. These discrepancies between experimental and calculated characteristic temperatures may originate from the systematic error on the absolute value of desorption temperatures on the theoretical side (variation with temperature of entropic terms for condensed phases and kinetic limitation of desorption have been neglected) and to the uncertainty of the pressure measurements on the experimental side.

Moreover, on the more regular sample (Figure 1b), the low-frequency side of the sharp band decreases in intensity between 473 and 573 K, resulting in the shift of its maximum from 3740 to 3750 cm^{-1} . This low-temperature feature may be related to phenomena not taken into account in the present work, such as interactions between OH groups and additional water molecules or with OH groups remaining on terraces. Nevertheless, the experimental trends observed above 573 K are well reproduced by calculations, thus enabling a validation of the picture of the surface as a function of temperature, as reported earlier.⁵⁶

4.2.3. Adsorption of Other Protic Molecules. Some of the features proposed in this model can be compared to experimental data on the adsorption of RH protic molecules (others than water) which protonate $\text{O}^{2-}_{\text{LC}}$ only thus avoiding the hydroxylation of $\text{Mg}^{2+}_{\text{LC}}$, and leading to simpler IR spectra. In addition to the expected bands growth, perturbation of the remaining OH bands is also observed (indeed, adsorption experiments on completely dehydroxylated surfaces are a challenge since they require high pretreatment temperatures). It is also assumed that the structure of the generated R^- does not modify the position of the expected bands. Within this hypothesis, Figure 9 depicts the calculated spectra.

Upon C_2H_2 ,²² H_2S ,^{22,95} NH_3 ²² and H_2 ^{22,96,97} adsorption, a band at 3712 cm^{-1} is observed instead of that at 3740 cm^{-1} . Gribov

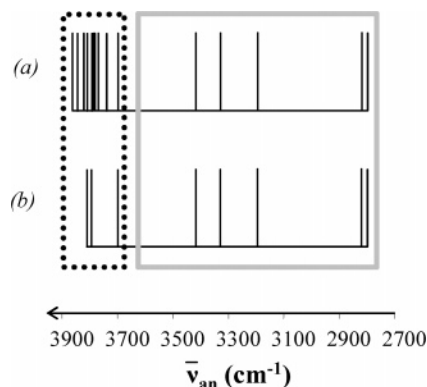


Figure 9. (a) Simulated IR spectra (cluster approach, B3LYP) of MgO powder hydroxylated at 10^{-2} Pa and 300 K. (b) Part of the spectrum associated with the protonated oxide ions $\text{O}^{2-}_{\text{LC}}$.

et al.⁹⁷ assigned this band to isolated $\text{O}_{3\text{C}}\text{-H}$, in agreement with calculations performed with small unembedded clusters,⁹⁸ whereas Knözinger et al.²² assigned it to multicoordinated isolated OH groups. These proposals are in line with the present work, as the high-frequency side of the sharp band is expected to exist only in the case of water dissociation, and its low-frequency side involves multicoordinated isolated OH groups on kinks or divacancies. Moreover, when N_2O (oxygen donor) is introduced after H_2 adsorption,⁹⁶ new bands at 3746 and 3762 cm^{-1} appear thus confirming that the high-frequency side of the sharp band is specific to hydroxyl adsorption on $\text{Mg}^{2+}_{\text{LC}}$. However, no conclusion can be made on the ability of a given $\text{Mg}^{2+}_{\text{LC}}\text{-O}^{2-}_{\text{LC}}$ to dissociate hydrogen or molecules others than water, so that no conclusion on the coordination (3, 4, and/or 5) of the protonated oxygen can be drawn here.

To conclude, the model proposed in Figure 5 for OH groups related to water dissociation is also suitable to assign the IR spectra obtained upon adsorption of other molecules, providing the respective acidities and the different nature of hydrogen-bonds are taken into account. This is another validation of the present work.

4.3. Synopsis: New Model for the Assignment of IR Spectra. None of the models of the literature (Table 1) leads to the same assignment of the spectra reported in Figure 5. The A, B, C, D terminology of Knözinger et al.²² can be used to propose a new model, but A hydroxyls have not been evidenced, and isolated and hydrogen-bond acceptors $\text{O}_{2\text{C}}\text{-H}$ are not taken into account in this terminology. The latter can thus be labeled as A' and C', respectively, because of the common origin with isolated and hydrogen-bond acceptors $\text{O}_{1\text{C}}\text{-H}$ (types A and C). Our new assignment of IR spectra is presented in Table 1. The high-frequency side of the sharp band involves monocoordinated hydrogen-bond acceptors hydroxyls (type C), whereas its low-frequency side involves multicoordinated isolated OH groups (type B) and dicoordinated hydroxyls (types A' and C'), never considered in the past to assign the spectra. The broad band is assigned to hydrogen-bond donor OH groups (type D).

As already mentioned, hydrogen-bonding is the first-order parameter to consider. Indeed, all hydrogen-bond donor OH

(96) Diwald, O.; Sterrer, M.; Knözinger, E. *Phys. Chem. Chem. Phys.* **2002**, *4*, 2811–2817.

(97) Gribov, E. N.; Bertarione, S.; Lamberti, C.; Spotto, G.; Zecchina, A. J. *Phys. Chem. B* **2004**, *108*, 16174–16186.

(98) Cavalleri, M.; Pelmenchikov, A.; Morosi, G.; Gamba, A.; Coluccia, S.; Martra, G. *Stud. Surf. Sci. Catal.* **2001**, *140*, 131–139.

(95) Deane, M.; Griffiths, D. L.; Lewis, I. A.; Winter, J. A.; Tench, A. J. *J. Chem. Soc., Faraday Trans. 1* **1975**, *71*, 1005–1012.

groups are characterized by a low frequency and correspond to the experimental broad band. These groups are, in practice, some of the $O_{3C}-H$ (corners), $O_{4C}-H$ (steps and corners), and $O_{5C}-H$ (valleys). On the contrary, hydrogen-bond acceptors, which are $O_{1C}-H$ and $O_{2C}-H$, correspond to the sharp band, involving also all isolated OH groups ($O_{2C}-H$, $O_{3C}-H$, and $O_{4C}-H$), contrary to the often admitted idea that only "linear" $O_{1C}-H$ are characterized by high frequencies. The model of Knözinger et al.²² is the nearest to ours: the wavenumbers related to hydrogen-bond donors and acceptors were already distinguished, although $O_{2C}-H$ was not considered, and A believed to exist at high desorption temperature.

The present model shows that the case of hydroxyl groups is somewhat more complex on MgO than on alumina, where vibrational frequencies were classified on the basis of hydrogen-bonding and oxygen coordination as first and second-order parameters, respectively.⁹ The present classification of OH groups may help interpret other spectroscopic or chemical properties of MgO powders.

5. Conclusion

Hydroxyl groups involving oxide and metal ions of low coordination on MgO surfaces have been modeled, and their stretching frequency has been evaluated thanks to periodic and cluster DFT calculations. The most important parameter determining the stretching frequency of a given type of OH group is hydrogen-bonding: isolated and hydrogen-bond acceptor OH groups exhibit significantly higher frequency than hydrogen-bond donor OH groups (see Figure 5). The second parameter to take into account is the location of OH groups in concave or convex areas of the surface, resulting in various interactions of the hydroxyl with its environment. The coordination of the oxygen of the hydroxyl appears to be a less important parameter.

The best agreement with experimental frequencies is obtained with the hybrid B3LYP exchange correlation functional, whereas the pure GGA PW91 functional leads to underestimate them, the relative band positions remaining however correct. Using the same functional, cluster and periodic models provide quite similar structural and vibrational results. Finally, it is important to take into account anharmonic effects.

The agreement between calculated thermal stabilities of OH groups, by means of a thermodynamic model, and those deduced

from experimental IR spectra acquired at increasing evacuation temperature, is found to be satisfactory and validates the choice of the systems used to describe irregularities on MgO. A new model has thus been proposed to help assign the main bands of IR spectra of hydroxylated MgO powders, taking into account hydrogen-bonding, local topology of surface sites, and the coordination of oxygen.

The assignments proposed can help identify hydroxyl groups involved in catalytic processes for example. The high catalytic activity of hydroxyl groups has indeed been evidenced by IR spectroscopy in the conversion of methylbutynol.¹⁶ The same experimental and DFT approach can be applied to 1H NMR⁹⁹ to identify the different types of OH groups and quantify those involved in basic reactivity.

This study illustrates how a systematic theoretical study of surface groups in very different topological environments can help assign experimental IR spectra. The use of several complementary description modes of the surface (periodic and clusters), the evaluation of the major calculation artifacts (by comparing different functionals), and finally the comparison of calculations with experimental data are required to quantify the influence of each factor (H-bonding character, topology, oxygen coordination, etc.) on the property investigated (stretching frequencies or chemical shifts). The approach proposed is expected to be valid for other oxides, which could shed some new light on the surface reactivity of oxide surfaces.

Acknowledgment. The authors wish to express their gratitude to David Loffreda of the Ecole Normale Supérieure de Lyon for explanations and much help in performing the anharmonic shift calculations. Hélène Lauron-Pernot and Dominique Costa from Laboratoire de Réactivité de Surface are also sincerely acknowledged for very interesting discussions. Most of the calculations were carried out at the IBM-SP at the CNRS-IDRIS computational centre, under Project No. 051847.

Supporting Information Available: Complete ref 74. This material is available free of charge via the Internet at <http://pubs.acs.org>.

JA068720E

(99) Chizallet, C.; Costentin, G.; Lauron-Pernot, H.; Maquet, J.; Che, M. *Appl. Catal. A* **2006**, *307*, 239–244.